Room temperature optoelectronic devices operating with spin crossover nanoparticles

Jean-Francois Dayen, Nikita Konstantinov, Marlène Palluel, Nathalie Daro, Bohdan Kundys, Mohamed Soliman, Guillaume Chastanet, Bernard Doudin

ARTICLE

Room temperature optoelectronic device operating with spin crossover nanoparticles

Received 00th January 20xx,
Accepted 00th January 20xx

DOI: 10.1039/x0xx00000x

Jean-Francois Dayen,[a,b] Nikita Konstantinov,[a] Marlène Palluel,[a,c] Nathalie Daro,[c] Bihdan Kundys,[a] Mohamed Soliman,[a] Guillaume Chastanet*[c] and Bernard Doudin*[a]

Molecular systems can exhibit multi-stimuli switching of their properties, with spin crossover materials having unique magnetic transition triggered by temperature and light, among others. Light-induced room temperature operation is however elusive, as optical changes between metastable spin states require cryogenic temperatures. Furthermore, electrical detection is hampered by the intrinsic low conductivity properties of these materials. We show here how a graphene underlayer reveals the light-induced heating that triggers a spin transition, paving the way to use these molecules for room temperature optoelectronics applications.

Introduction

Over the past decade, molecular electronics has become a major field of study for the development of alternative nanotechnology approaches to traditional silicon based electronics[1–3]. Among the large molecules library, spin crossover (SCO) molecules have garnered increasing attention as molecular switch building blocks for data storage, imaging, photodetection, energy harvesting and thermal applications[4–7]. The SCO molecular systems constitute a class of materials for which the transition metal centers can exhibit a transition between two different magnetic states resulting in modification of their physical properties: volume, dielectric constant, optical absorption and related properties... For the most studied Fe(II)-based SCO complexes, this switch occurs between a diamagnetic low spin (LS), most commonly stable at low temperatures, and a paramagnetic high spin (HS) state, usually stable at high temperatures. Interestingly, the spin-state transition can be triggered by different means including pressure, temperature, electric field or light. Moreover, the transition temperature can possibly exceed 300K, which positions SCO materials as interesting systems to realize room temperature molecular switches for the next generation of data storage and processing technologies.

Significant progress has been realized in the last years towards the integration of these materials into electrical devices[5,7]. The most popular approach to date consists in interconnecting the SCO compounds in between metallic electrodes to transduce electrically their thermal spin transition upon thermal variation of the SCO compound[8–12]. Devices are however limited by the intrinsic low electrical conductivity of SCO materials. One way to circumvent this issue is the use of a graphene substrate, of conductivity modified by the electrostatic environment change created by the phase switching of an adjacent SCO material. This concept was pioneered by Dugay et al. for layers of SCO nanoparticles[13], and recently by Geest et al. for SCO single crystals[14], where the authors showed how the conductance of a graphene sub or ad layer is modified under temperature-induced phase transition of the SCO.

Implementing the functionality of an optical commutation of the SCO spin state is obviously of upmost interest. Photoexcitation of the LS→HS (respectively HS→LS) transition, also referred as Light-Induced Excited Spin State Trapping (LIESST, respectively reverse-LIESST), is well documented[15]. The electrical detection of LIESST and reversed-LIESST in SCO thin films by means of a graphene detector was recently demonstrated by Konstantinov et al.[16], achieving the first resistive transduction of reversible LIESST functionality. The energy landscape allowing isothermal light stabilization of a metastable state limits however this process to low temperatures, typically below 60K, exceptionally reaching 130K[17], with Arrhenius law limiting the time stability of the light-triggered metastable state. Another promising alternative to realize photo-switching of SCO materials

In this report, we demonstrate a simple fabrication route and the operation of a hybrid optoelectronic device based on spin crossover Nanoparticles/Graphene (SCO/Gr) heterostructures (**Figure 1a**). Here, we take advantage of the multifunctionality of the SCO/Gr hybrid system to realize optoelectronic switching at room temperature by means of photothermal induced spin transition. Photon irradiation locally and quickly heats the sample and promote sa photo-assisted thermal spin crossover[15,18,19], opening the possibility of spin state manipulation with light at temperatures only limited by the transition temperatures of the SCO. If the LS ⇸ HS transition temperature is high enough and room temperature is within the thermal hysteresis loop, the cooldown of the sample after irradiation allows us to retain the photo-induced HS state at the

[a] Université de Strasbourg, CNRS, Institut de Physique et Chimie des Matériaux de Strasbourg (IPCMS), UMR 7504, 23 rue du Loess, Strasbourg, 67034, (France).
[b] Institut Universitaire de France (IUF), 1 rue Descartes, 75231 Paris cedex 05, (France).
[c] CNRS, Univ. Bordeaux, Bordeaux INP, ICMCB, UMR 5026, 87 av. Dr. A. Schweitzer, F-33600 Pessac (France)

* guillaume.chastanet@icmcb.cnrs.fr
* bernard.doudin@ipcms.unistra.fr

operating (room) temperature. While this observation was claimed to be possible, it has never been reported to date. Here, both thermal and optical addressability of the spin state by electrical detection means are demonstrated, with multiple non-volatile conductance states encoded into the graphene transistor conductivity upon tuning light excitation parameters. These results illustrate how SCO/Gr hybrid can capture in a single device the multifunctional properties of SCO molecular systems and the tunable electrical properties of graphene in a range of temperature suitable for applications, by means of a physical process compatible with fast operations requests.

Experimental

Synthesis procedure

The synthesis procedure of $[Fe(Htrz)_2(trz)](PF_6)$ is adapted from a previously reported protocol[18] and consists first in an anion exchange between the SO_4^{2-} of the $FeSO_4$ salt and the PF_6^- of the KPF_6 to give $Fe(PF_6)_2$ followed by its reaction with the triazole ligand. $FeSO_4$ (16 mmol) and the KPF_6 (32 mmol) are dissolved in water (14 mL) with a small amount of ascorbic acid to prevent oxidation of the Fe(II). The overall is stirred at 80 °C for 2 h 30 leading to a light green solution. After cooling to room temperature, 16 mL ethanol is added (16 mL) to precipitate the K_2SO_4 and the solution is stirred one hour more. The precipitate of K_2SO_4 is removed from the $Fe(PF_6)$ solution by filtration and washed once with about 50 mL of ethanol. The filtrated solution is cooled down to 5°C during 1 h to favor the precipitation of the remained solubilized K_2SO_4 and further filtrated and washed with ethanol (16 mL). This operation is repeated one more time. Then, a solution of Htrz (16 mmol) in ethanol (14 mL) is added dropwise to the $Fe(PF_6)_2$ solution with magnetic stirring and reflux at 80 °C under N_2 atmosphere. After 15 min, a white suspension is obtained and let to cool down at 5°C during 1 h to promote precipitation. The precipitate is separated by centrifugation (12 000 rcf, 5 minutes) and washed twice with ethanol and once with diethyl ether (with 50 mL each time). After drying at RT under ambient atmosphere overnight a white powder is obtained. Expected formula $[Fe(Htrz)_2(trz)](PF_6)$: C (17.71%), H (1.98%), N (30.97%), Fe (13.72%), P (7.61%); experimental values C (16.56%), H (2.04%), N (27.92%), Fe (11.81%), P (7.97%). The slight difference between the theoretical and experimental values might come most probably from the presence of K_2SO_4 impurity. Indeed, introducing 0.25 K_2SO_4 in the composition leads to C (15.99%), H (1.79%), N (27.98%), Fe (12.39%), P (6.87%) values that are much closer to the experimental ones.

Magnetic measurements

Magnetic measurements were performed using a Vibrating Sample Magnetometer from MicroSense EZ7, operating at 15 kOe and at 2 K min^{-1}. The diamagnetic contributions of the sample and the sample holder were removed from the data.

Device elaboration

The electric detector device is made of a monolayer of graphene grown by Chemical Vapor Deposition (CVD) and transferred on SiO_2(300nm)/Si substrate, with an active channel 300 µm wide and

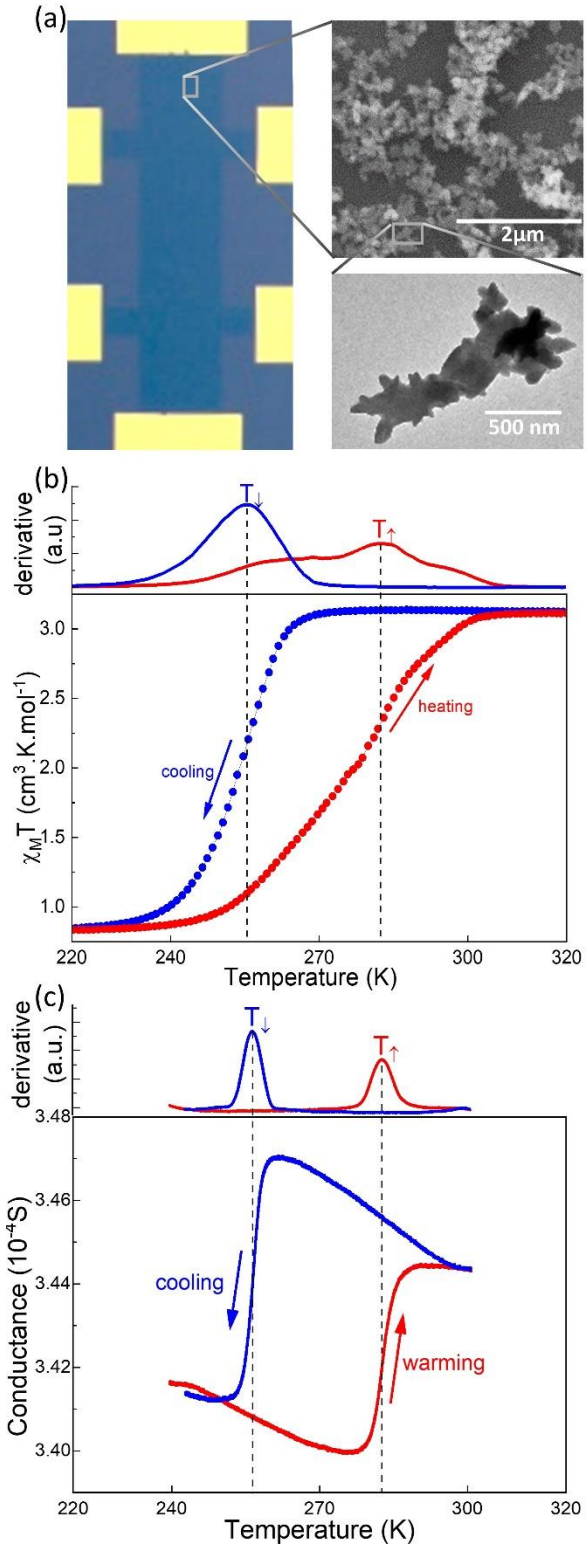

Figure 1: a) Picture of the device together with TEM image of the nanoparticles after synthesis (bottom right) and SEM image after deposition onto the graphene layer (top right). b) Thermal dependence of the $\chi_M T$ product with the derivative of the curve (top) of the nanoparticles as synthesized. c) Thermal dependence of the graphene conductance and the derivative curve (top).

1.5 mm long defined by etching through a resist patterned by laser lithography. A subsequent lithography step is used to define Au contacts, making possible transverse and longitudinal measurements of the sample conductance. In this work, we only use the end contacts as source and drain electrodes in a three terminals control of a field effect transistor where the gate electrode is the connected p-doped Si substrate.

The SCO nanoparticles are then dispersed in ethanol and put into an ultrasonic bath for around 20 min to disperse them well. The obtained solution is slightly pink. One to four droplets of this solution are then drop cast on the graphene surface, covering the Gr layer and providing proximity between the optically active SCO nanoparticles and the Gr sensor. Optical and SEM pictures of the final device are depicted in **Figure 1a**. The planar geometry of the device enables simple and direct optical access to the SCO material.

Photo-transport measurements were carried out in a He-flow cryostat. A dual channel high precision source meter K2634B and a K2182A nanovoltmeter were used for DC measurements. A Coherent OBIS LX laser (wavelength 647 nm, fluence 550 μW/mm^2) was used to irradiate the sample. The light was sent down to the sample using an optical fiber mounted in the optoelectronic measurement stick.

Transmission and Scanning electron microscopies

Transmission electron microscopy (TEM) images were acquired using a JEOL 1400+ (Japan), with a tension of 60 kV. Due to the aggregation and the non-specific morphology of the particles, only a rough estimation of the size can be given. Scanning electron microscopy (SEM) images were acquired using a JEOL 6700F (field emission gun) with a high-resolution mode. Experimental conditions were the followings: tension of 5 kV, working distance WD = 6 mm, probe current = 7 A and magnification of 500, 5 000, 10 000, 20 000 and 50 000.

Results and discussion

The particles obtained are analyzed by transmission electron microscopy. **Figure 1a** reports a picture of these particles showing elongated nanoparticles of about 200 nm length and 50 nm width, strongly agglomerated. This morphology corresponds to the one observed in the extensively investigated [Fe(Htrz)$_2$(trz)](BF$_4$) analog that exhibits a huge thermal hysteresis above 350 K[19,20,21].

These nanoparticles are characterized using magnetometry (**Figure 1b**). The thermal evolution of the molar magnetic susceptibility χ_M times the temperature clearly evidences the presence of a hysteresis loop. Upon warming from 200 K to 350 K, the χ_MT product increases from 0.83 cm^3 K mol^{-1} to 3.11 cm^3 K mol^{-1}. This indicates the thermo-induced LS to HS spin crossover. The fact that the χ_MT value at low temperature is not zero as expected agrees well with the presence of nanoparticles. Indeed, paramagnetic residue is often reported at the nanoscale[23]. This switching occurs at T↑ = 278 K, T↑ being the temperature at the middle of the transition in warming. Upon cooling from 360 K to 200 K, the χ_MT product decreases and recovers its initial value at 200 K witnessing the reversibility of the process. This switching in cooling mode occurs at T↓ = 254 K.

Successful electrical transduction of the SCO spin state is first validated by conductance (G) *vs* temperature (T) measurements (**Figure 1c**). Clear signatures of the electrical detection by the graphene layer of the thermally-induced spin transition of the SCO particles are manifested by a well-marked hysteresis in the conductance *vs* temperature curve that matches the magnetic thermal hysteresis (**Figures 1b and 1c**), and is not expected in pristine graphene [22,23] The transition temperatures (corresponding to a 50% fraction of HS species) are estimated by using the derivative plot dG /dT (Figure 2.b), at T↓ = 256 K in the cooling mode and at T↑ = 282 K in the heating mode (ΔT = 26 K). The thermal switching characteristics of the film match within a few K those of the nanoparticles powder extracted from magnetic measurements (**Figure 1b** T↑ = 278 K, T↓ = 254 K). This demonstrates the sensitivity of graphene to the magnetic molecular state of SCO compounds and confirms the report on continuous film of SCO nanoparticles by Dugay et al. [13]. Note that a more abrupt change of the graphene/SCO conductance signal upon spin transition compared to bulk material magnetic signal is observed. This may be attributed to a narrower size distribution of NP assembly promoted by drop casting process (dilution in ethanol, followed by the selection of the top part of the colloidal solution), compared to the raw NP powder used for magnetic measurements.

Photo-switching at temperatures just below the LS→HS transition can be triggered by means of light-induced heating, following

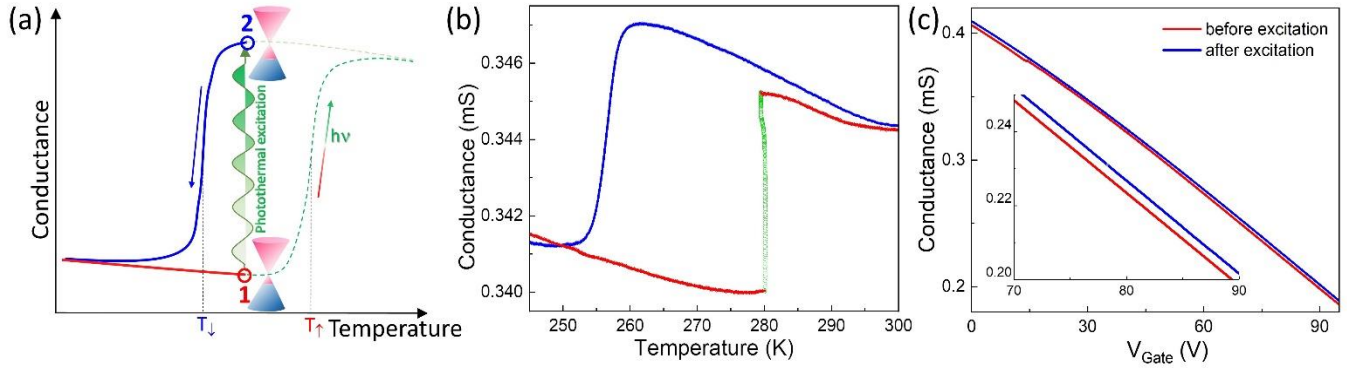

Figure 2. a) Schematics of the principle of thermally light-induced switching: an initial LS state **1** at temperature T experiences heating by photothermal excitation at temperatures exceeding T↑, and stabilizes in the HS state **2** when brought back to T less than T↓. b) Electrical detection of the light-induced switching, at T= 280 K (green dots), under red light illumination (λ = 647 nm, 550 μW/mm^2). c) Transfer curve of the graphene device in the two states, showing a heavily doped p graphene, slightly de-doped when the SCO is in the HS state.

previous reports using optical excitation and detection methods [24,25]. Cooperativity makes the thermal transition of the SCO often hysteretic, opening the possibility of writing and erasing magnetic states. For a LS low temperature phase system, the LS→HS transition temperature T↑ when heating up the system will be higher than the HS→LS transition temperature T↓ when cooling down. If the photo-irradiation is performed within the thermal hysteresis of the SCO compound, i.e. at temperatures T↓<T<T↑ when heating up (preparing the system in state **1**, in majority LS), the heat brought by light irradiation triggers the transition to state **2**, in majority HS, which remains stable when thermal equilibrium is re-established after switching off the light (**Figure 2a**). The written HS state is then stored as long as the temperature remains larger than T↓ , near T↑. For SCO materials of high-enough transition temperatures, ambient temperature operation can then be implemented. We unveil here how photo-thermal excitation can be used to optically write at room temperature a remote HS state into the SCO compound that can be transduced electrically into a low impedance signal by the three terminals graphene sensor.

Because it can be seen as an atomically thin two dimensional electron gas directly exposed to its environment, graphene is considered as an ideal sensor material. The graphene conductance can demonstrate modulation in response to change in its electrostatic environment. Spin crossover materials are known to experience a change in their dielectric permittivity, related to the change of charge configuration, upon switching.[26,27] Therefore, the most plausible scenario is that upon photothermal LS→HS transition, electrostatic changes in the SCO NP act as a 'molecular gate effect',[14,28] tuning the doping density of the graphene layer and as a consequence its conductance level. Such mechanism has recently been proposed as being responsible for the electrical transduction by graphene sensor of thermal spin transition into SCO single crystal[14] and SCO molecular thin film [16] based heterostructures.

To photo-thermally induce the LS→HS molecular switching, a red light (λ_1 = 647 nm, fluence 550 µW/mm^2) is used to irradiate the SCO particles. This wavelength has been chosen to ensure a photon energy smaller than the energy of the trap states at the graphene/silica interface, for sake of avoiding contribution from photogating effect[29,30] while still being within the wide absorption peak of the molecules. The absorption of the light by the heterostructure is used to induce sample heating responsible for the LS→HS transition of the SCO nanoparticles. Here, the photo-reversibility was not explored since the reverse-LIESST process was not reported on such compounds and the use of reverse photothermal effect has been argued to be difficult to implement.[31] Device measurements shown in **Figure 2b** follow the photo-thermal process demonstrated by previously reported optical experiments on powder samples [24,25,32,27]. The sample, first prepared in its LS state out of the hysteresis cycle below T↓ (left red part of the G(T) curve starting from 240 K), is then brought in the G(T) hysteresis region near room temperature (at 280 K), where it is irradiated for a few minutes (~ 5 to 10). At this given fixed temperature (280 K), the device clearly exhibits a change of electrical properties that mirrors the conductance change observed under thermal transition of the SCO. It therefore successfully provides an electrical response to the light-induced switching.

We can also take advantage of the gating electrode to investigate how the transfer curve of the transistor is modified by the transition from the LS to the HS states of the SCO nanoparticles. The graphene detector is significantly hole doped, due to its CVD process and adsorption of SCO materials. Its transfer curve is shifted (**Figure 2c**) towards increased hole doping levels-which clearly indicates that the switching of the SCO molecular state modifies the electronic state of the graphene, probably resulting from the modulation of the SCO dielectric properties upon spin state transition[14,16,32]

We also performed complementary experiments, in order to test the stability of the light-generated states. Varying the duration of the photo-thermal excitation allows to encode several conductive states, while tuning the proportion of the SCO population optically switched from the LS to HS state (**Figure 3**). In order to get insight into the tunability and stability of these photoconduction states, we expose the SCO/Gr device to incremental sequences of 1 minute-long photoexcitation followed by 5 minutes of relaxation in the dark (**Figure 3a**). We observe that each additional excitation results in a new conductive state. We assume that it results from the increase of the SCO population in the HS state as a result of longer photo-excitation. After 5 minutes of cumulated photoexcitation, all the SCO molecules have converted, and the device conductance gets saturated. These photo-excited states can be written at any temperature within the hysteresis as shown on **Figure 3b**, and

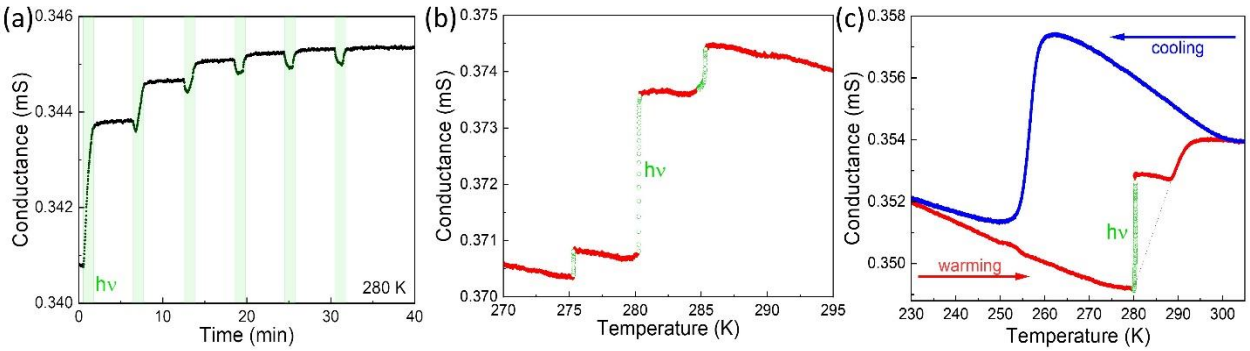

Figure 3. a) Successive photo-induced change of conductance (green areas) of the Gr/SCO device, exponentially approaching a stabilized 100 % HS state b) Stabilization of intermediate HS states by performing 1 min irradiation (in green) at several different temperatures within the thermal hysteresis loop. c) Sample prepared in the LS state at 280K, irradiated during 1 min, with related heating of around 10K, with a resulting partial occurrence of HS, stable in the temperature range 280 < T< 290K. Dotted red curve shows the conductance vs temperature while heating without irradiation.

illustrate a very good thermal stability inside the hysteresis region, which is an asset of the molecular state switching of the photo-thermally excited population. Furthermore, short-enough irradiation makes clear the related heating of the sample (**Figure 3c**), further illustrating how partial HS states can be generated and stabilized within the thermal hysteresis loop.

Conclusion

We presented concluding evidence of the electrical detection of the photo-thermal switching of SCO nanoparticles at temperatures only limited by the spin transition temperatures of the material, making room temperature operation possible. This results in a multifunctional optoelectronic switch that combines the bistability of SCO compounds and the gate-tunable low electrical impedance of graphene. Isothermal stability allows to encode optically different analogic remote states, while controlling the proportion of SCO molecules populating the HS state upon tuning the duration and the temperature of the light excitation. The HS and LS conductive states, can also be addressed and reset by thermal sweep out of the hysteresis region (below $T_{\downarrow}$, and over $T_{\uparrow}$). The presented results also pave the way to a realistic implementation of SCO molecular materials for optoelectronics. Nanoparticles have optimal size range for applications relevance. They are large enough to ensure cooperativity, key to hysteresis properties. They are small enough to minimize the switching time, avoiding a nucleation propagation process. Time resolved fast optical studies indeed showed that switching occurs at time scale below the ns and thermal recovery can occur in the 10 -100 ns range [26,27,33]. In our case, much longer heating time scales are needed with our continuous power source, most probably due the large scale of our device and the needed higher illumination power and absorption efficiency of our system. The need of higher irradiation powers could be mitigated by materials design, for example by means of the synthesis of hybrid nanoparticles incorporating a strong optical absorber[35], or by appropriate electrode geometry.[36,37] The tunability by design of a graphene detector, combined with its high mobility , make possible device integration in reasonably fast electronics. Realistic improvements of the hybrid device should result in significantly higher sensitivity, while bringing the graphene sensor closer to the charge neutrality as well as depositing more controlled thin nanoparticles ensemble. These results therefore open new prospects for the applicability of magnetic molecular switches in optoelectronic data recording and phase change memory devices.[38]

Conflicts of interest

There are no conflicts to declare.

Acknowledgements

We thank Marc Ziegler and Olivier Cregut for technical assistance in using the Ti-sapphire laser, and Fabien Chevrier for cryogenics. The financial support from the Agence Nationale de la Recherche (HEROES ANR-17-CE09-0010-01, MIXES ANR-19-CE09-0028) is acknowledged as well as the CNRS, University of Bordeaux, and Nouvelle Aquitaine Region. This work of the Interdisciplinary Thematic Institute QMat, as part of the ITI 2021 2028 program of the University of Strasbourg, CNRS and Inserm, was supported by IdEx Unistra (ANR 10 IDEX 0002), and by SFRI STRAT'US project (ANR 20 SFRI 0012) and EUR (QMat-ANR-18-EUR-0016) under the framework of the French Investments for the Future Program. The authors acknowledge the use of cleanroom facilities from the STnano platform. J.-F. D. thanks the Institut Universitaire de France (IUF) for financial support. The UMS PLACAMAT is acknowledged for the TEM facilities more specifically Marion Gayot for her help.

Notes and references

1 N. Fuentes, A. Martín-Lasanta, L. Álvarez De Cienfuegos, M. Ribagorda, A. Parra and J. M. Cuerva, *Nanoscale*, 2011, **3**, 4003–4014.

2 B. L. Feringa, *J. Org. Chem.*, 2007, 72, 6635–6652.

3 S. Jan Van Der Molen and P. Liljeroth, *J. Phys. Condens. Matter*, 2010, 22, 30.

4 A. Bousseksou, G. Molnár, L. Salmon and W. Nicolazzi, *Chem. Soc. Rev.*, 2011, **40**, 3313–3335.

5 K. Senthil Kumar and M. Ruben, *Coord. Chem. Rev.*, 2017, **346**, 176–205.

6 P. Gütlich and Y. Garcia, in *Reference Module in Chemistry, Molecular Sciences and Chemical Engineering*, Elsevier, 2015.

7 G. Molnár, S. Rat, L. Salmon, W. Nicolazzi and A. Bousseksou, *Adv. Mater.*, , DOI:10.1002/adma.201703862.

8 E. A. Osorio, K. Moth-Poulsen, H. S. J. Van Der Zant, J. Paaske, P. Hedegård, K. Flensberg, J. Bendix and T. Bjørnholm, *Nano Lett.*, 2010, **10**, 105–110.

9 F. Prins, M. Monrabal-Capilla, E. A. Osorio, E. Coronado and H. S. J. Van Der Zant, *Adv. Mater.*, 2011, **23**, 1545–1549.

10 E. J. Devid, P. N. Martinho, M. V. Kamalakar, I. Šalitroš, Ú. Prendergast, J. F. Dayen, V. Meded, T. Lemma, R. González-Prieto, F. Evers, T. E. Keyes, M. Ruben, B. Doudin and S. J. Van Der Molen, *ACS Nano*, 2015, **9**, 4496–4507.

11 A. Rotaru, J. Dugay, R. P. Tan, I. A. Guralskiy, L. Salmon, P. Demont, J. Carrey, G. Molnár, M. Respaud and A. Bousseksou, *Adv. Mater.*, 2013, **25**, 1745–1749.

12 S. K. Karuppannan, A. Martín-Rodríguez, E. Ruiz, P. Harding, D. J. Harding, X. Yu, A. Tadich, B. Cowie, D. Qi and C. A. Nijhuis, *Chem. Sci.*, , DOI:10.1039/d0sc04555a.

13 J. Dugay, M. Aarts, M. Giménez-Marqués, T. Kozlova, H. W. Zandbergen, E. Coronado and H. S. J. van der Zant, *Nano Lett.*, 2017, **17**, 186–193.

14 E. P. Geest, K. Shakouri, W. Fu, V. Robert, V. Tudor, S. Bonnet and G. F. Schneider, *Adv. Mater.*, 2020, **32**, 1903575.

15 G. Chastanet, M. Lorenc, R. Bertoni and C. Desplanches, *Comptes Rendus Chim.*, 2018, 21, 1075–1094.

16 N. Konstantinov, A. Tauzin, U. N. Noumbé, D. Dragoe, B. Kundys, H. Majjad, A. Brosseau, M. Lenertz, A. Singh, S. Berciaud, M.-L. Boillot, B. Doudin, T. Mallah and J.-F. Dayen, *J. Mater. Chem. C*, 2021, **9**, 2712–2720.

17 S. Hayami, Z. Z. Gu, Y. Einaga, Y. Kobayasi, Y. Ishikawa, Y. Yamada, A. Fujishima and O. Sato, *Inorg. Chem.*, 2001, **40**, 3240–3242.

18 K. H. Sugiyarto and H. A. Goodwin, *Aust. J. Chem.*, 1994, **47**, 263–277.

19 O. Kahn, J. Kröber and C. Jay, *Adv. Mater.*, 1992, **4**, 718–728.

20 L. Salmon and L. Catala, *Comptes Rendus Chim.*, 2018, **21**, 1230–1269.

21 L. Moulet, N. Daro, C. Etrillard, J.-F. Létard, A. Grosjean and P. Guionneau, *Magnetochemistry*, 2016, **2**, 10.

22 S. Das Sarma, S. Adam, E. H. Hwang and E. Rossi, *Rev. Mod. Phys.*, 2011, **83**, 407–470.

23 J. Heo, H. J. Chung, S. H. Lee, H. Yang, D. H. Seo, J. K. Shin, U. I. Chung, S. Seo, E. H. Hwang and S. Das Sarma, *Phys. Rev. B - Condens. Matter Mater. Phys.*, 2011, **84**, 035421.

24 W. Hellel, A. Ould Hamouda, J. Degert, J. F. Létard and E. Freysz, *Appl. Phys. Lett.*, 2013, **103**, 143304.

25 S. Bonhommeau, G. Molnár, A. Galet, A. Zwick, J. A. Real, J. J. McGarvey and A. Bousseksou, *Angew. Chemie - Int. Ed.*, 2005, **44**, 4069–4073.

26 S. Bonhommeau, T. Guillon, L. M. Lawson Daku, P. Demont, J. S. Costa, J. F. Létard, G. Molnár and A. Bousseksou, *Angew. Chemie - Int. Ed.*, 2006, **45**, 1625–1629.

27 A. Bousseksou, G. Molnár, P. Demont and J. Menegotto, *J. Mater. Chem.*, 2003, **13**, 2069–2071.

28 A. Mahmood, C. S. Yang, S. Jang, L. Routaboul, H. Chang, A. Ghisolfi, P. Braunstein, L. Bernard, T. Verduci, J. F. Dayen, P. Samorì, J. O. Lee and B. Doudin, *Nanoscale*, 2019, **11**, 19705–19712.

29 G. Cao, X. Liu, Y. Zhang, W. Liu, M. Deng, G. Chen, G. Zhang, Q. Li, L. G. Beka, X. Li and X. Wang, *ACS Appl. Mater. Interfaces*, 2019, **11**, 12170–12178.

30 Y. D. Kim, M. H. Bae, J. T. Seo, Y. S. Kim, H. Kim, J. H. Lee, J. R. Ahn, S. W. Lee, S. H. Chun and Y. D. Park, *ACS Nano*, 2013, **7**, 5850–5857.

31 M. Castro, O. Roubeau, L. Piñeiro-López, J. A. Real and J. A. Rodríguez-Velamazán, *J. Phys. Chem. C*, 2005, **119**, 17334–17343.

32 A. Iazzolino, G. Galle, J. Degert, J. F. Létard and E. Freysz, *Chem. Phys. Lett.*, 2015, **641**, 14–19.

33 K. Ridier, A. Bas, V. Shalabaeva, W. Nicolazzi, L. Salmon, G. Molnár, A. Bousseksou, M. Lorenc, R. Bertoni, E. Collet and H. Cailleau, *Adv. Mater.*, 2019, **31**, 1901361.

34 G. Gallé, C. Etrillard, J. Degert, F. Guillaume, J. F. Létard and E. Freysz, *Appl. Phys. Lett.*, 2013, **102**, 063302.

35 M. Palluel, N. M. Tran, N. Daro, S. Buffière, S. Mornet, E. Freysz and G. Chastanet, *Adv. Funct. Mater.*, 2020, **30**, 2000447.

36 P. Rastogi, A. Chu, C. Gréboval, J. Qu, U. N. Noumbé, S. S. Chee, M. Goyal, A. Khalili, X. Z. Xu, H. Cruguel, S. Ithurria, B. Gallas, J. F. Dayen, L. Dudy, M. G. Silly, G. Patriarche, A. Degiron, G. Vincent and E. Lhuillier, *Nano Lett.*, 2020, **20**, 3999–4006.

37 U. N. Noumbé, C. Gréboval, C. Livache, A. Chu, H. Majjad, L. E. Parra López, L. D. N. Mouafo, B. Doudin, S. Berciaud, J. Chaste, A. Ouerghi, E. Lhuillier and J.-F. Dayen, *ACS Nano*, 2020, 14(4), 4567–4576.

38 T. K. Ekanayaka, G. Hao, A. Mosey, A. S. Dale, X. Jiang, A. J. Yost, K. R. Sapkota, G. T. Wang, J. Zhang, A. T. N'Diaye, A. Marshall, R. Cheng, A. Naeemi, X. Xu and P. A. Dowben, *Magnetochemistry*, 2021, **7**, 37.